



HAL
open science

Complete genome of the Medicago anthracnose fungus, *Colletotrichum destructivum*, reveals a mini-chromosome-like region within a core chromosome

Nicolas Lapalu, Adeline Simon, Antoine Lu, Peter-Louis Plaumann, Joëlle Amselem, Sandrine Pigné, Annie Auger, Christian Koch, Jean-Félix Dallery, Richard J O'Connell

► To cite this version:

Nicolas Lapalu, Adeline Simon, Antoine Lu, Peter-Louis Plaumann, Joëlle Amselem, et al.. Complete genome of the Medicago anthracnose fungus, *Colletotrichum destructivum*, reveals a mini-chromosome-like region within a core chromosome. *Microbial Genomics*, 2024, 10 (8). hal-04683720

HAL Id: hal-04683720

<https://hal.inrae.fr/hal-04683720v1>

Submitted on 2 Sep 2024

HAL is a multi-disciplinary open access archive for the deposit and dissemination of scientific research documents, whether they are published or not. The documents may come from teaching and research institutions in France or abroad, or from public or private research centers.

L'archive ouverte pluridisciplinaire **HAL**, est destinée au dépôt et à la diffusion de documents scientifiques de niveau recherche, publiés ou non, émanant des établissements d'enseignement et de recherche français ou étrangers, des laboratoires publics ou privés.



Distributed under a Creative Commons Attribution 4.0 International License

1 Complete genome of the *Medicago* anthracnose fungus,
2 *Colletotrichum destructivum*, reveals a mini-chromosome-like
3 region within a core chromosome

4 Nicolas Lapalu^{1§}, Adeline Simon^{1§}, Antoine Lu¹, Peter-Louis Plaumann², Joëlle Amselem³,
5 Sandrine Pigné¹, Annie Auger¹, Christian Koch², Jean-Félix Dallery^{1#}, Richard J. O'Connell^{1#}

6 ¹ Université Paris-Saclay, INRAE, UR BIOGER, 91120 Palaiseau, France

7 ² Division of Biochemistry, Department of Biology, Friedrich-Alexander-Universität Erlangen-
8 Nürnberg, 91058 Erlangen, Germany

9 ³ Université Paris-Saclay, INRAE, URGI, 78000 Versailles, France

10 [§] These authors contributed equally.

11 **# Corresponding authors:** Richard J. O'Connell, richard.oconnell@inrae.fr; Jean-Félix Dallery jean-
12 felix.dallery@inrae.fr.

13 **Keywords:** fungal genomics; accessory chromosome; chromosome rearrangements; segmental
14 duplication; phytopathogenic fungus, *Medicago truncatula*.

15 **Repositories:** GEO GSE246592; NCBI BioProject PRJNA1029933.

16 **Abbreviations:** AT: acyltransferase domain; AR: accessory region; BDBH: bidirectional best hit; BGC:
17 biosynthetic genes cluster; CAT: conidial anastomosis tubes; CAZyme: carbohydrate active enzyme;
18 CDS: coding sequence; CE: carbohydrate esterase; Chr: chromosome; DNA: deoxyribonucleic acid; GH:
19 glycoside hydrolase; GO: gene ontology; HCT: horizontal chromosome transfer; HPI: hours post-
20 inoculation; KS: ketosynthase domain; LINE: long interspersed nuclear element; LTR: long terminal
21 repeats; MITE: miniature inverted-repeat transposable element; NRPS: non-ribosomal peptide
22 synthetase; PCA: principal component analysis; PCP: peptidyl carrier protein domain; PCR: polymerase
23 chain reaction; PFGE: pulsed-field gel electrophoresis; PKS: polyketide synthase; PL: polysaccharide
24 lyase; RBH: reciprocal best hit; RFP: red fluorescent protein; RNA: ribonucleic acid; SD: segmental
25 duplication; SMKG: secondary metabolism key gene; SMRT: single molecule real time; TE: transposable
26 element; TIR: terminal inverted repeat; TPM: transcript per million.

27 **Abstract**

28 *Colletotrichum destructivum* (*Cd*) is a phytopathogenic fungus causing significant economic losses on
29 forage legume crops (*Medicago* and *Trifolium* species) worldwide. To gain insights into the genetic



This work is licensed under a CC-BY 4.0 license. <https://creativecommons.org/licenses/by/4.0/>
A CC-BY public copyright license has been applied by the authors to the present document and will be applied to all subsequent versions up to the Author Accepted Manuscript arising from this submission, in accordance with the grant's open access conditions.

30 basis of fungal virulence and host specificity, we sequenced the genome of an isolate from *M. sativa*
31 using long-read (PacBio) technology. The resulting genome assembly has a total length of 51.7 Mb and
32 comprises 10 core chromosomes and two accessory chromosomes, all of which were sequenced from
33 telomere to telomere. A total of 15,631 gene models were predicted, including genes encoding
34 potentially pathogenicity-related proteins such as candidate secreted effectors (484), secondary
35 metabolism key enzymes (110) and carbohydrate-active enzymes (619). Synteny analysis revealed
36 extensive structural rearrangements in the genome of *Cd* relative to the closely-related Brassicaceae
37 pathogen, *C. higginsianum*. In addition, a 1.2 Mb species-specific region was detected within the
38 largest core chromosome of *Cd* that has all the characteristics of fungal accessory chromosomes
39 (transposon-rich, gene-poor, distinct codon usage), providing evidence for exchange between these
40 two genomic compartments. This region was also unique in having undergone extensive intra-
41 chromosomal segmental duplications. Our findings provide insights into the evolution of accessory
42 regions and possible mechanisms for generating genetic diversity in this asexual fungal pathogen.

43 Impact statement

44 *Colletotrichum* is a large genus of fungal phytopathogens that cause major economic losses on a wide
45 range of crop plants throughout the world. These pathogens vary widely in their host specificity and
46 may have either broad or narrow host ranges. Here, we report the first complete genome of the alfalfa
47 (*Medicago sativa*) pathogen, *Colletotrichum destructivum*, which will facilitate the genomic analysis of
48 host adaptation and comparison with other members of the *Destructivum* species complex. We
49 identified a species-specific 1.2 Mb region within chromosome 1 displaying all the hallmarks of fungal
50 accessory chromosomes, which may have arisen through the integration of a mini-chromosome into a
51 core chromosome and could be linked to the pathogenicity of this fungus. We show this region is also
52 a focus for segmental duplications, which may contribute to generating genetic diversity for adaptive
53 evolution. Finally, we report infection by this fungus of the model legume, *Medicago truncatula*,
54 providing a novel pathosystem for studying fungal-plant interactions.

55 Data summary

56 All RNA-seq data were submitted to the NCBI GEO portal under the GEO accession GSE246592.
57 *C. destructivum* genome assembly and annotation are available under the NCBI BioProject
58 PRJNA1029933 with sequence accessions CP137305-CP137317.

59 Supplementary data (genomic and annotation files, genome browser) are available from the INRAE
60 BIOGER Bioinformatics platform (<https://bioinfo.bioger.inrae.fr/>). Transposable Elements consensus
61 sequences are also available from the French national data repository, research.data.gouv.fr with doi
62 10.57745/TOO1JS.

63 Introduction

64 The ascomycete fungal pathogen *Colletotrichum destructivum*, causes anthracnose disease on lucerne
65 (alfalfa, *Medicago sativa*) and *Trifolium* species and is responsible for significant economic losses on
66 these forage legumes [1, 2]. Despite being isolated most frequently from members of the Fabaceae, *C.*
67 *destructivum* has occasionally been recorded from genera of the Asteraceae (*Helianthus*, *Crupina*),
68 Poaceae (*Phragmites*) and Polygonaceae (*Rumex*) [3, 4]. It has a worldwide distribution that includes
69 the USA, Canada, Argentina, Italy, Netherlands, Greece, Serbia, Morocco, Saudi Arabia, and Korea. *C.*

70 *destructivum* is a haploid fungus with no known sexual stage [3]. Previous reports of a sexual stage
71 (*Glomerella glycines*) for soybean isolates of *C. destructivum* [5, 6] were based on incorrect
72 identification of the soybean pathogen, which was recently shown to be *C. sojae* [7].

73 Over the last decade, the application of multi-locus molecular phylogeny approaches has revealed that
74 *C. destructivum* belongs to the *Destructivum* species complex, which contains 17 accepted taxa [3, 8].
75 All these plant pathogenic species show distinct host preferences, spanning phylogenetically diverse
76 botanical families. An increasing number of species in the *Destructivum* complex have now been
77 genome sequenced, namely *C. higginsianum* [9, 10], *C. tanacetii* [11], *C. lentis* [12] and *C. shisoi* [8],
78 which cause disease on Brassicaceae, *Tanacetum* (Asteraceae), *Lens* (Fabaceae) and *Perilla*
79 (Lamiaceae), respectively. The clade therefore provides excellent opportunities for comparative
80 genomic studies on the genetic determinants of host adaptation.

81 The availability of complete genome sequences is crucial not only for the analysis of large gene clusters,
82 such as secondary metabolism biosynthetic gene clusters, but also for understanding fungal genome
83 evolution. Complete or near-complete genome sequences have enabled the structure and dynamics
84 of accessory mini-chromosomes to be analyzed in several *Colletotrichum* species [9, 13, 14]. The
85 importance of mini-chromosomes for virulence on plant hosts has been demonstrated in several fungal
86 pathogens including *Fusarium oxysporum* f.sp. *lycopersici* [15], *Magnaporthe oryzae* [16], *C. lentis* [12]
87 and *C. higginsianum* [17].

88 Here, we present the complete genome sequence and gene annotation of *C. destructivum* strain LARS
89 709, hereafter called *Cd709*, based on long-read sequencing with PacBio Single Molecule, Real-Time
90 (SMRT) Sequel technology. The resulting high-quality chromosome-level assembly allowed us to
91 perform comparative genomics with the close sister species, *C. higginsianum*, highlighting gene
92 content specificity and extensive genomic rearrangements. In particular, the genome showed evidence
93 of multiple segmental duplications, as well as the likely integration of a mini-chromosome into one
94 core chromosome. Although the origin of this integrated region remains to be determined, it displays
95 all the hallmarks of fungal mini-chromosomes. We also show for the first time that *C. destructivum* is
96 pathogenic, and completes its life-cycle, on the model plant *Medicago truncatula*, providing a new
97 tractable pathosystem in which both partners have been genome-sequenced.

98 Materials and Methods

99 **Fungal and plant materials**

100 The *C. destructivum* strains used in this study were originally isolated from *M. sativa* in Saudi Arabia
101 (CBS 520.97, LARS 709) and Morocco (CBS 511.97, LARS 202) [2], and are hereafter called *Cd709* and
102 *Cd202*. The *C. higginsianum* strains used for comparative genome and chromosome analyses were IMI
103 349063A and MAFF 305635 [10, 17, 18], hereafter called *Ch63* and *Ch35*, respectively. The fungi were
104 cultured as described previously [18].

105 Seeds of nine *M. truncatula* accessions (Table S1) were provided by the INRAE Centre de Ressources
106 Biologiques *Medicago truncatula* (UMR 1097, Montpellier, France), while *M. sativa* seeds were
107 purchased from Germ'line SAS (France). *M. truncatula* seeds were first abraded with sandpaper and
108 imbibed with water for 1 h before sowing in seed compost (Floragard Vertriebs-GmbH, Oldenburg,
109 Germany), while *M. sativa* seeds were sown directly in the same compost. All plants were grown in a
110 controlled environment chamber (23°C day, 21°C night, 12-h photoperiod, PPFR 110 $\mu\text{mol}\cdot\text{m}^{-2}\cdot\text{s}^{-1}$).

111 **Infection assays and microscopy**

112 To test the susceptibility of *M. truncatula* accessions to *Cd709*, intact plants (17-days-old) were
113 inoculated by first immersing the above-ground parts in a solution of 0.01 % (v/v) Silwet to wet the
114 leaves, then by immersion in a suspension of *C. destructivum* spores ($2 \times 10^6 \text{ ml}^{-1}$). The inoculated plants
115 were incubated in a humid box inside a controlled environment chamber (25°C, 12-h photoperiod,
116 PPFR $40 \mu\text{mol m}^{-2} \text{ s}^{-1}$). For microscopic examination, pieces of infected tissues were cleared with a 1:3
117 mixture of chloroform:ethanol for 1h, then with lactophenol for 30 min, before mounting on a
118 microscope slide in 70 % glycerol and imaging with a Leica DM5500 light microscope. Symptoms were
119 recorded at 4 dpi.

120 **Pulsed-field gel electrophoresis (PFGE) and Southern blotting**

121 The plugs containing the conidial protoplasts for PFGE were prepared as previously described [17].
122 Pulsed-field gel electrophoresis (Bio-rad CHEF-DR II system) was performed using the following
123 conditions: Runtime 260 hours; Switch time 1200 s to 4800 s; 1.5 V / cm; 0.75 x TBE at 8°C. Yeast
124 chromosomal DNA served as size marker (BioRad; 200 kb – 2 Mb).

125 Southern blotting was conducted using standard protocols [19]. A digoxigenin labeled probe was
126 generated by PCR following the manufacturer's instructions (PCR DIG Probe Synthesis Kit, Roche). The
127 993 bp probe (*Cd709* chr1, position 6,711,095 to 6,712,088) was specific to mini-chromosome-like
128 sequences at the right arm of chromosome 1 in *Cd709*. Hybridization was performed in DIG Easy Hyb
129 buffer at 42°C overnight. The membrane was then extensively washed with low and high stringency
130 buffers and subsequently blocked with buffer B2 (1% Blocking powder [Roche] in buffer B1 [100 mM
131 Maleic acid, 150 mM NaCl, pH 7.5]). The blocking solution was then replaced with antibody solution
132 (buffer B2 containing DIG-antibody 1:26,000 (Roche)). The membrane was washed with buffer B1
133 containing 0.3% Tween20. The membrane was subsequently equilibrated in buffer B3 (100 mM Tris
134 pH 9.5, 100 mM NaCl, 50 mM MgCl_2) and developed with chemiluminescence (CDP-Star, Roche).

135 **Genome data, assembly, rearrangements and duplications**

136 The genomic DNA of *Cd709* was used to prepare a size-selected library (20kb) prior to sequencing with
137 a PacBio Sequel sequencer (kit 2.1, Keygene N.V., Wageningen, The Netherlands) on two SMRT cells,
138 yielding raw data with approximately 224 X genome coverage (1.474.759 reads, N50 10.837 bp).
139 Genome assemblies were generated from several runs of the Hierarchical Genome-Assembly Process
140 version 4 (HGAP4) and Canu [20] assemblers. The draft genome was polished with the Arrow algorithm
141 and the completeness of the assembly was evaluated with BUSCO using the Ascomycota gene set as
142 evidence [21]. Telomeres were validated by the presence of at least three repeats of the
143 TTAGGG/CCCTAA motif at the end of assembled contigs [22]. The polished assembly was aligned with
144 nucmer against the *Ch63* and *Ch35-RFP* genomes to visualize chromosome rearrangements.
145 SDDetector [9] was used to detect segmental duplications in combination with Bedtools and BWA-
146 MEM for validation. The *Cd709* mitochondrial genome was assembled with Organelle_PBA [23] (Table
147 S2).

148 **Transcriptome data and analysis**

149 RNA sequencing was performed on samples of mRNA from undifferentiated mycelium grown
150 axenically and two different stages of plant infection, 48 and 72 h after inoculation, corresponding to
151 the biotrophic and necrotrophic phase, respectively. Mycelium was grown for three days in potato

152 dextrose liquid medium (PDB, Difco) at 25°C with shaking (150 rpm) and harvested by filtration.
153 Seedlings of *M. sativa* (eight days old) were inoculated by placing a droplet (10 µl) of *Cd709* spore
154 suspension (7×10^5 spores/ml) onto the surface of each cotyledon and the plants were then incubated
155 as described for *M. truncatula*. Discs of infected cotyledon tissue were harvested using a cork borer (4
156 mm diameter). After grinding the tissues in liquid nitrogen, total RNA was extracted using the RNeasy
157 plant mini kit (Qiagen). Libraries were then prepared from each sample type using the TruSeq Paired-
158 end Stranded mRNA Kit and sequenced (100 bp reads) using a HiSeq4000 sequencing platform
159 (IntegraGen Genomics, Evry, France). RNA-Seq paired reads were cleaned and trimmed using
160 Trimmomatic [24] and then mapped to the genome assembly of *Cd709* using STAR [25]. A genome-
161 guided transcript assembly was obtained from mappings with StingTie v1.3.4. Assembled raw
162 transcripts were then filtered based on the TPM distribution per transcript per library.

163 **Genome annotation**

164 Transposable elements (TE) were searched in the *C. destructivum* genome sequence using the REPET
165 package [26, 27]. Consensus sequences identified with the TEde novo pipeline were classified using the
166 PASTEC tool [28], based on the Wicker hierarchical TE classification system [29], and then manually
167 filtered and corrected. The resulting library of consensus sequences was used to annotate TE copies in
168 the whole genome using the TEannot pipeline.

169 Protein-coding genes were annotated using the Eugene [30] and FunGAP [31] tools. Predicted genes
170 were filtered out when 10% of their CDS overlapped a Transposable Element predicted by the REPET
171 package. Filtered predicted genes from Eugene and FunGAP were clustered together based on their
172 CDS coordinates (overlap of one base required) with no strand consideration. The Annotation Edit
173 Distance (AED) [32] was computed with transcript and protein evidence for each transcript and the
174 predicted model with the best score was retained at each locus. Mitochondrial genomes were
175 annotated with MFannot [33] and MITOS2 [34]. Results were manually inspected and in case of
176 divergence between the predictions, the longer gene model was retained.

177 The synteny between *C. destructivum* and *C. higginsianum* proteomes was analysed with SynChro [35]
178 which detects ortholog proteins with Reciprocal Best Hit (RBH), based on 40% similarity and a length
179 ratio of 1.3. Colinear orthologs were then grouped in syntenic blocks, according to a delta threshold =
180 1 (very stringent mode). Non-syntenic blocks were extracted when five or more consecutive non-
181 syntenic genes were found. Proteome similarities with other *Colletotrichum* spp. were performed with
182 Blast 2.2.28+ and the results filtered with a cut-off of 30% identity and 50% query coverage. Proteome
183 synteny and associated figures were obtained using Clinker [36].

184 **Functional annotation of predicted genes**

185 Functional annotations of genes obtained using Interproscan 5.0 [37] and Blastp (e-value $<1e-5$) [38]
186 against the NCBI nr databank (September 2019) were then used to perform Gene Ontology [39]
187 annotation with Blast2GO [40]. Carbohydrate active enzymes (CAZymes) were annotated with dbCAN2
188 [41] launching HMMER, Diamond and Hotpep against dedicated databases. Genes were considered as
189 CAZymes when at least 2 of the three tools provided a positive annotation.

190 Genes encoding potential secreted proteins were predicted with a combination of SignalP v4.1 [42],
191 TargetP v1.1 [43] and TMHMM v2.0 [44] results. The secretome was defined as the union of SignalP
192 and TargetP results and then intersected with TMHMM results (0 or only 1 transmembrane domain).

193 Proteins smaller than 300 amino acids were then extracted and considered as Small Secreted Proteins
194 (SPPs). In parallel, EffectorP v2.0 [45] was applied to the predicted secretome to identify putative
195 effector proteins. Finally, the intersection of EffectorP and SPPs results was retained to establish a list
196 of potential effectors.

197 To detect secondary metabolism biosynthetic gene clusters (BGCs), predicted genes were submitted
198 to antiSMASH (Antibiotics and Secondary Metabolite Analysis Shell) v5 [46]. Only core biosynthetic
199 genes (commonly known as secondary metabolism key genes, SMKGs) were considered for further
200 analysis. Presence/absence patterns of SMKGs were based on reciprocal best hits with *Ch63* and *Ch35*,
201 and then manually inspected. Among the newly predicted secondary metabolism key genes (SMKGs),
202 those encoding polyketide synthases (PKS) and non-ribosomal peptide synthases (NRPS) were checked
203 for the presence of the minimal expected set of enzymatic domains, namely KS and AT domains for
204 PKS, and A and PCP domains for NRPS. Terpene synthases and dimethylallyltryptophan synthase
205 (DMATS) genes were manually inspected and retained if they had RNA-seq or protein support. Those
206 *Cd709* genes not predicted as SMKGs by antiSMASH, but orthologous to a *C. higginsianum* SMKG were
207 also included. For example, antiSMASH failed to annotate six terpene synthase (TS) that are present in
208 both species.

209 **Codon usage analysis**

210 Codon usage was computed for predicted gene coding sequences (CDS) on each chromosome or region
211 using the EMBOSS tool 'cusp'. The resulting codon usage matrix (i.e. the fraction of each codon in a
212 given amino acid) was subjected to Fisher's exact tests (with a Bonferroni correction for multiple
213 testing) to address the statistical significance of differences between the core and mini-chromosomes.
214 The matrix was also subjected to a Principal Component Analysis (PCA) and the results were projected
215 onto the first two principal components. To analyse the GC percentage of the three letters of each
216 codon, the 'cusp' tool was run individually on each CDS of each chromosome or region and the results
217 were represented as density plots. The corresponding figures were generated using R (v. 4.0.5) and
218 the libraries ggplot2 (v. 3.3.3), cowplot (v.1.1.1) and ggbeeswarm (v. 0.6.0), all available from the CRAN
219 repository (<https://cran.r-project.org/>).

220 Results

221 **A novel *Colletotrichum destructivum* - *Medicago truncatula* pathosystem**

222 The cell biology of infection of *M. sativa* by *C. destructivum* isolate 709 (*Cd709*) was previously
223 described [2]. Here, we report infection of the model plant *M. truncatula* (barrel medic) by this species.
224 Five out of the nine tested *M. truncatula* accessions, including the genome-sequenced accession
225 ESP074-A [47], were found to be susceptible to *C. destructivum* in two independent infection assays
226 (Fig. 1, Table S1). At 4 days post inoculation (dpi), necrotic water-soaked lesions were visible on the
227 trifoliolate leaves of the susceptible accessions (Fig. 1). In contrast, the leaves of resistant accessions
228 presented only small necrotic flecks or no visible symptoms. The genome-sequenced accession R108-
229 C3, which is widely used for *M. truncatula* functional genomics [48], was resistant to *C. destructivum*
230 in these infection assays.

231 On cotyledons of the susceptible *M. truncatula* accession ESP155-D, *Cd709* spores germinated to form
232 melanized appressoria, which by 48 hpi had penetrated host epidermal cells to form bulbous,

233 intracellular biotrophic hyphae that were confined to the first infected cell (Fig. 2a). Thinner
234 necrotrophic hyphae started to emerge from the tips of the biotrophic hyphae at 60 hpi (Fig. 2b), and
235 after 72 hpi the fungus had completed its asexual cycle by producing sporulating structures (acervuli)
236 on the surface of the dead tissues (Fig. 2c). On cotyledons of the resistant accession ESP163-E,
237 appressoria formed abundantly on the leaf surface but penetrated host epidermal cells very
238 infrequently (Fig. 2d, e). Groups of dead epidermal cells underlying the appressoria appeared yellow-
239 brown in colour and had granulated contents, suggesting they had undergone a hypersensitive cell
240 death response. Rarely, small hyphae were visible in epidermal cells beneath appressoria but they
241 developed only a short distance into the dead cells and most remained smaller than the appressorium.
242 Acervuli were never observed on plants of accession ESP163-E.

243 **Genome assembly and structural annotation**

244 Long-read data allowed us to generate a complete genome assembly for *Cd709*, with a total length of
245 51.75 Mb in which all 12 chromosomes were sequenced from telomere to telomere (Fig. 3), together
246 with the circular mitochondrial genome (34 kb). Annotation of transposable elements revealed a total
247 of 49 consensus sequences, representing all the possible TEs in the *Cd709* genome. Classification of
248 the TEs (Table S3) showed that the genome contains 18 different families of retrotransposons,
249 including eleven LTR (Long Terminal Repeats) and seven LINE (long interspersed nuclear element), 28
250 DNA transposons, including 25 TIR (terminal inverted repeat), one helitron and two MITE (Miniature
251 Inverted-Repeat Transposable Elements), as well as three unclassified repeated elements. The library
252 of 49 consensus sequences was then used to annotate TE copies in the *Cd709* genome. Overall, TEs
253 covered 6.2 % of the genome assembly by length. The Class I LTR Gypsy superfamily was the most
254 abundant in terms of coverage and number of copies, whereas the Class I TIR Tc1-Mariner was the
255 most abundant in terms of full-length copies. Two Gypsy transposons (R172 and G87) resemble the
256 most abundant TE family in *C. higginsianum*, namely the LTR transposon family RLX_R119 [9]. Looking
257 at the distribution of TE families along the chromosomes, we found that the telomeres of all twelve *C.*
258 *destructivum* chromosomes were associated with a single copy of a TE belonging to the helitron family
259 (G103).

260 To annotate the protein-coding genes, a genome-guided assembly of RNA-Seq reads provided 16,122,
261 13,901 and 15,081 transcripts for axenic mycelium, 48 hpi and 72 hpi libraries, respectively (Table S4),
262 with 1.88 TPM, 9.38 TPM and 4.90 TPM as minimum expression levels, respectively (Fig. S1).
263 Assembled transcripts were then used to predict gene models in conjunction with *Colletotrichum* and
264 Ascomycota protein databanks. The results of EuGene and FunGap were combined and filtered to
265 generate the *Cd709* gene set comprising 15,631 complete gene models, of which 11,853 had transcript
266 support and 15,172 resembled Ascomycota predicted proteins. Features of the gene annotation are
267 summarized in Table S5. The completeness of this annotation was confirmed by comparison to the
268 BUSCO Ascomycota set (1,315 genes), with 1,309 complete genes predicted and only one missing.
269 Functional annotation assigned InterPro entries to 10,298 genes, among which 7,475 had at least one
270 GO term and 1,105 were potential enzymes (annotated with an Enzyme Code). Based on Blast2GO
271 descriptions, 12,192 predicted genes (78%) had a predicted function, i.e. a description other than
272 “hypothetical protein” (Table S6 tab ‘All’). The mitochondrial genome of *Cd709* was annotated with 29
273 tRNAs, 2 rRNAs (small and long subunit) and 21 genes.

274 **Plant interaction-related genes**

275 A total of 619 *Cd709* genes were annotated to encode CAZymes, among which 410 were assigned to
276 the Glycoside Hydrolase (GH), Carbohydrate Esterase (CE) and Polysaccharide Lyase (PL) CAZyme
277 classes (Table S6 tab 'CAZyme'). The proportion of genes in each CAZyme class closely resembled that
278 previously found in *Ch63* [49], and 98% (400/410) of *Cd709* CAZyme genes were also detected in the
279 *Ch63* genome. *In silico* analysis of the *Cd709* secretome revealed a total of 2,608 potential extracellular
280 secreted proteins, including 1,118 small proteins (<300 amino acids). Among these, 484 genes were
281 retained as putative effectors because they were also present among 508 genes identified by EffectorP.
282 Comparing these to the effector repertoire of *Ch63*, a total of 127 putative effectors (26.2%) were
283 unique to *Cd709*, having no Reciprocal Best Blast Hit in *Ch63* (Table S6 tab 'Predicted effectors'). A total
284 of 110 secondary metabolism key genes (SMKGs) were detected in the *Cd709* genome using the fungal
285 version of antiSMASH and were manually curated. These *C. destructivum* SMKGs were compared to
286 the 105 *C. higginsianum* SMKGs [9]. Overall, 78 % (94 out of 120) of the SMKGs were present in both
287 species (Table S6 tab 'Secondary metabolism', Fig. S2). A total of 17 *C. destructivum* SMKGs, distributed
288 over eight BGCs, were not detected in *C. higginsianum*.

289 **Chromosome structure comparison**

290 Complete chromosome-level assemblies are available for two different *C. higginsianum* strains,
291 namely IMI 349063A (*Ch63*) [9] and MAFF 305635-RFP (*Ch35-RFP*), a transformant of MAFF 305635
292 (*Ch35*) expressing red fluorescent protein which lacks both mini-chromosomes 11 and 12 [10, 17]. The
293 genetic proximity of *C. destructivum* and *C. higginsianum* allowed us to align assemblies to observe
294 chromosome structural variations. This generated 38 Mb of *C. destructivum* alignments (>10 kb) with
295 each *C. higginsianum* strain, ranging from 88 to 96.7% identity. Thus, *C. destructivum* shared
296 approximately 73.6 % of its total genome length with *C. higginsianum*. At the chromosome scale,
297 alignments revealed that five chromosomes of *C. destructivum* (chr1, 2, 3, 5 and 9) were not involved
298 in any large rearrangements, five others (chr4, 6, 7, 8 and 10) showed inter-chromosomal
299 rearrangements, while the two mini-chromosomes (chr11 and 12) lacked large regions of conserved
300 sequences and appear to be species specific (Fig. 4A).

301 One rearrangement involved chr7 and chr8 of *Cd709* resulting in chr4 and chr10 of *Ch63*. The break-
302 points in chr7 and chr8 were associated with TEs in *Cd709* (Fig. S3 A and B). A similar rearrangement
303 was found relative to *Ch35-RFP*, albeit with different break-points in both species that were not
304 associated with TEs (Fig. S3 F and G). A second rearrangement involved chr4 and chr10 of *Cd709* such
305 that their left and right arms result in chr9 and chr7 of *Ch63*, respectively (Fig. S3 C and D). Interestingly
306 this rearrangement was not found relative to *Ch35-RFP*, suggesting that it is specific to particular
307 *C. higginsianum* strains, as was noted previously [10]. A third inter-chromosomal rearrangement
308 concerned 121 kb at the 5' extremity of *Cd709* chr6 coming from chr4 and contig_1 of *Ch63* and *Ch35-*
309 *RFP*, respectively. In *C. destructivum*, this break-point is surrounded by TEs and non-syntenic regions
310 (Fig. S3 E). Remarkably, a specific rearrangement of 42 kb between chr11 of *Cd709* and contig 11 of
311 *Ch35-RFP* (Fig. S3 H) corresponds to a region that is absent from the *Ch63* genome assembly and which
312 encodes highly variable effectors (having \leq 90% alignment coverage) and secondary metabolism-
313 related proteins [10]. In addition, several short stretches (2 to 5 kb in length) from chr11 of *Cd709* were
314 present at the extremities of chromosome 6 in *Ch63* and the corresponding region of *Ch35-RFP* (contig
315 _9) (Fig. 4).

316 A notable feature of the *C. destructivum* genome assembly is the unusually large size of chr1 (7.3 Mb),
317 which is 0.9 Mb longer than the largest chromosome in *C. higginsianum* (6.4 Mb). Genome alignments
318 highlighted a near-complete synteny between chr1 of *Cd709* and chr2 of *Ch63* except for a 1.2 Mb
319 subtelomeric region (coordinates chr1:6076875-7282542), for which no similarity was found in *C.*
320 *higginsianum* (Fig. 4). Synteny between the genes of *Cd709* and those of *Ch63* was investigated using
321 SynChro. With stringent settings, 400 syntenic blocks were identified based on 12,135 Reciprocal Best
322 Hits. A total of 1,083 genes were found in 47 non-syntenic blocks composed of at least five consecutive
323 *Cd709*-specific genes (Tables S7 & S8). The largest non-syntenic block, corresponding to the 1.2 Mb
324 region specific to *Cd709* on chr1, contained 305 genes. Mini-chromosome chr12 contained one non-
325 syntenic block of 170 genes, while chr11 was divided into seven non-syntenic blocks, the largest
326 containing 106 genes. Although only 356/1,083 genes inside non-syntenic blocks could be annotated
327 with a GO term, GO enrichment tests revealed that the *Cd709*-specific genes were enriched in protein
328 kinases, protein phosphorylation activity and secondary metabolism process (Table S9). Likewise,
329 effector genes were found to be enriched in non-syntenic blocks whereas CAZymes were depleted
330 (Table S10).

331 **Validation of the 1.2 Mb non-syntenic region in *C. destructivum* chromosome 1**

332 To verify the large non-syntenic region identified within chr1, we first checked for potential errors in
333 the sequence assembly of this region by manually inspecting long reads spanning the two junctions
334 (Fig. S4). Secondly, to obtain an assembly-independent validation, pulsed-field gel electrophoresis
335 (PFGE) and a Southern hybridization were performed (Fig. 5A, B). A 993 nt probe (coordinates chr1:
336 6,711,095 to 6,712,088) was designed within the 1Mb non-syntenic region to target a unique locus
337 that avoided TEs (Fig. 5B). This probe is 83.5% identical to the gene CH63R_14488 located on
338 chromosome 11 of *Ch63* that was used as a hybridization control.

339 Chromosomes of two *C. destructivum* isolates (*Cd709* and *Cd202*) and two *C. higginsianum* isolates
340 (*Ch63* and *Ch35*) were separated by PFGE and analysed by Southern hybridization (Fig. 5C, D). For both
341 *C. destructivum* isolates, the probe hybridized to molecules with high molecular weight that could
342 correspond to the largest chromosome, consistent with a location on chr1 (Fig. 5C, D). The high
343 molecular weight signals were absent in the *C. higginsianum* blots, and instead hybridization signals
344 were detected at a position corresponding to mini-chromosome 11, although these were weak, as
345 expected for a probe with only 83.5% identity to the target. Overall, our findings validate that a non-
346 syntenic region is embedded within chr1 of *C. destructivum*. Hereafter, we refer to the syntenic and
347 non-syntenic portions as chr1A and chr1B, respectively, and their distinct properties were explored
348 further in the following analyses.

349 **Region chr1B shows the characteristic features of fungal accessory chromosomes**

350 In many aspects, the region chr1B of *Cd709* resembled the mini-chromosomes 11 and 12. All three
351 compartments were more AT-rich than the core genome. Region chr1B was also highly enriched with
352 TEs, having 32.8 % coverage with TE copies by length, similar to chr11 and chr12 (32.3 and 35.1 %,
353 respectively), whereas the core chromosomes (excluding chr1B) had only 3 to 6.2 % TE coverage (Table
354 1, Fig. 3, Table S11). Moreover, the distribution of TE families in region 1B and the two mini-
355 chromosomes differed markedly from the core chromosomes in that they were all enriched with LINE
356 retrotransposons (44 %, 19 % and 34 % coverage, respectively), compared to only 7 % in the core
357 genome (Table 3). LINE TEs are also present in *C. higginsianum* on mini-chromosomes 11 and 12, but

358 their expansion was less striking in this species (7 % and 2 % coverage, respectively) (Fig. S5) than in
359 *Cd709* [9].

360 Examination of the gene content of region chr1B revealed that, similar to the mini-chromosomes, it
361 was overall depleted in protein-coding genes (2-fold less than the core chromosomes), contained a
362 significantly larger proportion of genes encoding proteins of unknown function (i.e. annotated as
363 hypothetical proteins), and had fewer expressed genes (RNA-seq transcript evidence) compared to the
364 core genome (Table 1). Considering categories of potentially pathogenicity-related genes, no CAZyme
365 genes or SMKGs were detected in either region chr1B or chr 12, although eight SMKGs were present
366 on chr11 (Table S6, Tab 'Secondary metabolism'), all of which had RNA-seq transcript support.
367 Moreover, 38 effectors were found in chr1B and the two mini-chromosomes. Remarkably, 36 of these
368 were absent from *C. higginsianum* (had no RBH in *Ch63*), of which 20 were expressed *in planta* (Table
369 S6 tab 'Predicted effectors'). With 15 and 10 effectors respectively, the mini-chromosomes 11 and 12
370 were significantly enriched in putative effectors compared to the core chromosomes whereas no
371 enrichment was observed for the 13 effectors of the chr1B (Table 1). Remarkably, the most highly
372 expressed effectors during the biotrophic phase (48 hpi), namely CDEST_01870 (chr1B) and
373 CDEST_15472 (chr12), were located on mini-chromosome-like regions. This raises the possibility that
374 genes carried in such regions are important for virulence.

375 **Codon usage in region chr1B and the mini-chromosomes differs from the core chromosomes**

376 Analyses of codon usage were used previously to detect differences between the core and accessory
377 chromosomes or lineage-specific compartments of other plant pathogenic fungi [15, 50, 51]. We
378 therefore computed the codon usage of CDS located on the core chromosomes, mini-chromosomes
379 and the chr1B region of *Cd709*. Based on a principal component analysis, codon usage on the core
380 chromosomes was very homogeneous, whereas that of the mini-chromosomes and region chr1B
381 clustered together and separately from the core chromosomes (Fig. 6A). To illustrate this in greater
382 detail, we plotted the codon usage for each amino acid and for each chromosome or region (Fig. S6,
383 representative examples are given for 3 amino acids in Fig. 6B). For these analyses, we excluded the
384 two amino acids (Trp and Met) that are encoded by a single codon. Based on Fisher's exact tests for
385 each of the remaining 59 codons, almost all the codon usages were different between the core
386 chromosomes on one hand and chr1B, chr11 or chr12 on the other hand. In striking contrast, there
387 were only three differential codon usages between chr1B and chr11 and one between chr1B and chr12.
388 However, chr11 and chr12 were most different from each other with 15 differential codons (Table S12;
389 adjusted $P < 0.001$).

390 **Region chr1B is a hotspot for segmental duplications**

391 The genome of *Cd709* was inspected for segmental duplications, as described previously for *C.*
392 *higginsianum* [9]. A total of 48 duplications involving genes were detected on four chromosomes (chr1,
393 chr6, chr11 and chr12). Among them, 12 duplications were larger than 10 kb (Fig. 7) of which only
394 three were inter-chromosomal (all involving chr12). Similar to *C. higginsianum* [9], these inter-
395 chromosomal duplications were all associated on at least one side with TEs, supporting a potential role
396 of TEs in duplication (Fig. S7). However, in contrast to *C. higginsianum*, these duplications did not take
397 place preferentially near telomeres.

398 A remarkable feature of region chr1B was that it showed a strong intra-chromosome duplication
399 pattern, with some regions replicated up to three times (Fig. 7). Assembling large duplications can be
400 difficult even with long-read sequences [52]. To check for possible bias during assembly, the eight
401 largest intra-chromosome duplications on chr1B were inspected manually (Table S13). Due to the
402 problem of multiple reads mapping to duplicated regions, we considered only uniquely mapped reads.
403 Consequently, the read-coverage of these eight regions was on average 2-fold lower than the non-
404 duplicated regions. No other regions of chr1B showed a significant decrease in coverage, and the
405 extremities of the SD regions were well-anchored to chr1B. Reads were identified spanning the two
406 smallest duplications, SD1B-2 (10 reads) and SD1B-6 (22 reads), but other duplicated regions were too
407 large (>16 kb) to be spanned by single PacBio reads. Finally, the short-read RNA-seq data used to
408 annotate the genome were also employed to detect mutations within the duplicated genes. Mutations
409 were detected in all the duplicated regions, albeit with support from only few reads in most cases.
410 Taken together, these results support the reliability of the observed duplications in region chr1B.

411 To gain insight into the possible origin of region chr1B, we examined conservation of the 300 genes
412 contained within this region in the genomes of 23 other *Colletotrichum* species (Table S14). As
413 expected, given that *C. destructivum* and *C. higginsianum* belong to the same species complex [3], the
414 total proteome of *Cd709* showed greatest similarity to that of *Ch63* (14,372 conserved proteins).
415 Surprisingly however, the chr1B proteome shared most conserved proteins with a phylogenetically
416 distant species, namely *C. truncatum* (217 protein matches, compared to only 134 matches in *C.*
417 *higginsianum*) [53]. Almost half of the genes shared with *C. truncatum* were involved in segmental
418 duplications within the *Cd709* chr1B. Remarkably, the region triplicated in SD1B-1, SD1B-3 and SD1B-
419 7 was also found in a large duplicated region represented by two contigs within the *C. truncatum*
420 genome assembly (Fig. S8) [54], which may be located on a mini-chromosome due to their low GC
421 content (49.0%, compared to 51.2% in the longer contigs of *C. truncatum*). Other genes located within
422 the *Cd709* SD1B-1 duplications had Blast matches that were mostly restricted to *C. incanum*, *C.*
423 *spaethianum* and *C. tofieldiae* (Spaethianum species complex), *C. salicis* and *C. nymphaeae* (Acutatum
424 species complex), *C. fructicola* (Gloeosporioides species complex), *C. sublineola* (Graminicola species
425 complex) and *C. orchidophilum*, which vary in their phylogenetic distance from *C. destructivum* [53].
426 The absence of these gene sequences from the *C. higginsianum* genome was confirmed by Tblastn
427 searches against the NCBI wgs Colletotrichum database (266 genomes).

428 Examination of the gene content in duplicated regions of chr1B gave few clues to their possible role in
429 the host interaction or the advantage for the fungus to maintain multiple mutated copies of these
430 genes. One gene duplicated four times (CDEST_01898, CDEST_01949, CDEST_02058 and
431 CDEST_02116) encoded a major facilitator superfamily transporter. The five genes duplicated between
432 SD1B-2 and SD1B-6 comprised four FAD-binding domain-containing proteins and a patatin-like serine
433 hydrolase.

434 Discussion

435 In this study, we present a chromosome-level reference assembly of the *C. destructivum* genome, a
436 phytopathogen causing anthracnose disease principally on species of *Medicago* and *Trifolium*
437 (Fabaceae). Among other members of the *Deconstructivum* species complex, which currently contains 17
438 recognised species [3], the genomes of *C. lentis*, *C. tanacetii* and *C. shisoi* were sequenced previously
439 but the resulting assemblies were highly fragmented, containing 2980, 5242 and 36,350 contigs,
440 respectively [8, 11, 12]. Using PacBio long-read sequencing, we were able to generate a gapless
441 assembly of the *Cd709* genome which, together with that of *Ch63* [9], provides a second complete

442 genome within the *Destructivum* species complex, facilitating future comparative genomic analyses
443 within this important group of plant pathogens.

444 Alignment of the *Cd709* genome assembly with those of *C. higginsianum* strains *Ch63* and *Ch35*
445 revealed large-scale chromosome rearrangements between the two closely-related species. Some of
446 these rearrangements were potentially mediated by recombination between homologous regions
447 containing TEs, which flanked one or both of the breakpoints. Similar TE-mediated chromosome
448 rearrangements were previously reported at the intra-species level in *C. higginsianum* [10]. Our
449 analysis of synteny between the genomes of *Cd709* and *Ch63* also revealed the presence of a 1.2 Mb
450 species-specific region within Chr1 of *Cd709*, which we called Chr1B. This ‘accessory region’ (AR)
451 displays many of the hallmarks that characterize fungal mini-chromosomes, or ‘accessory
452 chromosomes’, in that it is AT-rich, transposon-rich, gene-poor and has a distinct codon usage [51, 55–
453 57]. In all these respects, Chr1B resembles the mini-chromosomes Chr11 and Chr12 but is strikingly
454 different from the rest of Chr1 and other core chromosomes of *Cd709*. The TE enrichment observed in
455 Chr1B and both mini-chromosomes is largely caused by the specific expansion of LINE and TIR elements
456 in these compartments, unlike the core chromosomes where the Gypsy TE family predominates.

457 Using PFGE and Southern hybridization with a probe specific to Chr1B, we were able to confirm that
458 this AR is carried not only on Chr1 of *Cd709* but also on the largest chromosome of *Cd202*, despite the
459 widely-separated geographical origins of these two isolates (Saudi Arabia and Morocco, respectively).
460 Analysis of a larger collection of *C. destructivum* isolates is now needed to determine the extent to
461 which Chr1B is conserved within this pathogen species. The presence of an AR embedded within a core
462 chromosome has been reported in other plant pathogenic fungi. For example, isolates of the T race of
463 *Cochliobolus heterostrophus* harbor an AR of about 1.2 Mb distributed between two core
464 chromosomes that contains the *Tox1* locus producing the T-toxin polyketide [58, 59]. In *Verticillium*
465 *dahliae*, Chr3 and Chr4 each harbor two ARs of ~300 kb [60], while in *Fusarium poae* a 204 kb block
466 with AR characteristics is inserted near one telomere of Chr3 [57]. However, it should be noted that in
467 these two examples the inserted AR blocks are 4- to 6-fold smaller than Chr1B of *Cd709*.

468 Our working hypothesis is that the AR Chr1B arose by the integration of a mini-chromosome into a
469 core chromosome of *C. destructivum*, but the mechanism by which this occurred is unclear. Despite
470 the subtelomeric position of Chr1B, its integration is unlikely to have resulted from the telomeric fusion
471 of a mini-chromosome with a core chromosome because it is flanked on both sides by portions of Chr1,
472 both of which are highly syntenic to Chr2 of *C. higginsianum*. A chromosome containing distinct regions
473 characteristic of core and accessory chromosomes was previously reported in the genome of *C.*
474 *fructicola* strain Nara gc5 [61]. In this case, the chimeric chromosome, called Nara_c11, is smaller (2.8
475 Mb) than *Cd709* chromosome 1 (7.3 Mb) and the TE-rich, gene-poor AR occupies most of the
476 chromosome (66 % by length), in contrast to *Cd709* Chr1B, which occupies only 16 %. A further
477 difference to *Cd709* Chr1B is that the AR of Nara_c11 includes a telomere, suggesting that in this case
478 the chimeric chromosome arose through a different mechanism. Taken together, our findings provide
479 further evidence for genetic exchange between core and accessory genomic compartments in
480 *Colletotrichum* species [61]. In other fungi, chromosome breakage-fusion-bridge (BFB) cycles have
481 been invoked not only in the creation of accessory chromosomes from core chromosomes [62], but
482 also in their reintegration into core chromosomes [63].

483 A distinguishing feature of the Chr1B AR is that it has undergone extensive region-specific segmental
484 duplications. Some inter-chromosomal SDs in *Cd709* were associated with TEs at one or both of their
485 borders, as we found previously in *Ch63* [9], but there was little evidence that the region-specific SDs
486 in Chr1B were mediated by TEs. Similarly, the AR of *C. fructicola* chromosome Nara_c11 was found to
487 be implicated in numerous intra- and inter-chromosomal SDs but as in *Cd709* these were not
488 consistently flanked by TEs [61]. Among fungal pathogens, SDs can play important roles in generating
489 genetic diversity and novel gene functions, either at the level of expression or coding sequence [64,
490 65]. A recent study on *Fusarium* strains infecting banana also highlighted the importance of SDs in
491 driving the evolution of ARs and the effector genes contained within them [66]. Although the *C.*
492 *destructivum* genome contains a complete Mat1-2-1 mating-type locus (Table S6, Tab MAT1-2-1), and
493 should therefore be capable of sexual reproduction, this has never been observed [67], [3]. In this
494 context, segmental duplication may therefore provide an important mechanism for generating genetic
495 diversity for host adaptation in this essentially asexual pathogen.

496 A remarkable finding was that some segmentally duplicated blocks of genes within Chr1B of *C.*
497 *destructivum* are conserved and syntenic with duplicated regions in the genome of *C. truncatum*, a
498 species that is phylogenetically very distant [53]. Given that these two taxa diverged ~60 million years
499 ago [68], soon after speciation in *Colletotrichum*, these SDs may be very ancient and have been
500 selectively retained in some species and lost in others. Alternatively, these duplicated regions may
501 have been acquired by horizontal chromosome transfer (HCT) from another species to a common
502 ancestor, or through independent transfers to *C. destructivum* and *C. truncatum*. HCT would be
503 consistent with the distinct codon bias in Chr1B and the taxonomic incongruity of many genes within
504 this region. The horizontal transfer of a mini-chromosome between vegetatively incompatible biotypes
505 of *C. gloeosporioides* was shown experimentally [69, 70], and it is well-documented that genetic
506 material can be exchanged following fusion between conidial anastomosis tubes of the same, or even
507 different, *Colletotrichum* species [71–73].

508 Chr1B contains a variety of genes with potential roles in fungal virulence, some of which were
509 expressed during infection. These include genes encoding 13 candidate secreted effector proteins, 8
510 protein kinases, 5 major facilitator superfamily membrane transporters, 5 heterokaryon
511 incompatibility (HET) proteins and 8 putative transcription factors (TFs) (Table S6). It is interesting to
512 note that, similar to Chr1B, the accessory ‘pathogenicity chromosome’ of *Fusarium oxysporum* f.sp.
513 *lycopersici* is enriched not only with effectors genes but also with genes encoding protein kinases,
514 membrane transporters, HET proteins and TFs, of which one TF was shown to regulate the expression
515 of plant-induced effector genes [74],[75]. TFs were also found to be enriched in the four lineage-
516 specific ARs of *V. dahliae* [60]. Overall, the gene content of Chr1B suggests that it may contribute to *C.*
517 *destructivum* pathogenicity. This was demonstrated experimentally for ARs in two other members of
518 the *Destructivum* species complex, namely Chr11 of *C. higginsianum* (isolate *Ch35*) which was essential
519 for virulence on *A. thaliana* [17], and Chr11 of *C. lentis*, which was required for virulence on lentil [12].
520 In the case of *Cd709*, it is noteworthy that the three most highly expressed and plant-induced effector
521 genes are all located in ARs, namely CDEST_01870 on Chr1B, CDEST_15404 on Chr11 and CDEST_15472
522 on Chr12. These and other pathogenicity-related genes carried within these genomic compartments
523 will provide interesting candidates for future functional analysis.

524 Finally, we show here that *Cd709* can complete its life cycle not only on its original host, *M. sativa*, but
525 also on the widely-studied model legume, *M. truncatula*. Until now, the only other *Colletotrichum*

526 species known to attack *M. truncatula* was *C. trifolii*, which belongs to the phylogenetically distant
527 Orbiculare species complex and uses a different infection process where the biotrophic phase extends
528 to many host cells [76, 77]. With complete genome assemblies and high-quality gene annotations
529 available for both partners, together with abundant genetic tools and resources on the plant side, the
530 *C. destructivum* - *M. truncatula* interaction could provide a tractable new model pathosystem for
531 studying hemibiotrophic fungal interactions with Fabaceae hosts. Our identification of susceptible and
532 resistant *M. truncatula* accessions also raises the possibility that natural variation among accessions
533 could be exploited to analyse the genetic basis of resistance to *C. destructivum* [78].

534 Conflicts of interest:

535 The authors declare that there are no conflicts of interest.

536 Funding:

537 This work was partly supported by funding from the Agence Nationale de la Recherche (ERA-CAPS grant
538 ANR-17-CAPS-0004-01) to R.J.O. The BIOGER unit benefits from the support of Saclay Plant Sciences-
539 SPS (ANR-17-EUR-0007). The Funders had no role in the study design, data analysis, data interpretation
540 or decision to publish.

541 Author contributions:

542 Conceptualization: NL, AS, CK, JFD, RJO; Investigation: PLP, SP, AA, RJO; Formal analysis: NL, AS, AL, JA,
543 JFD; Visualization: NL, AS, PLP, JA, CK, JFD, RJO; Writing – Original Draft: NL, AS, PLP, JA, CK, JFD, RJO;
544 Writing – Review & Editing: NL, AS, CK, JFD, RJO; Supervision: NL, CK, RJO; Funding acquisition: RJO.

545 Acknowledgements:

546 We are grateful to the following bioinformatics platforms and partners for providing help and/or
547 computing and/or storage resources: Genotoul bioinformatics platform Toulouse Occitanie (Bioinfo
548 Genotoul, doi: 10.15454/1.5572369328961167E12), CATI BARIC (<https://www.cesgo.org/catibaric/>),
549 and INRAE-LIPME Bioinfo (Sébastien Carrère). We also thank Dr Alexander Wittenberg (KeyGene
550 N.V., The Netherlands) for help with sequencing, and the INRAE Centre de Ressources Biologiques
551 *Medicago truncatula* for providing seeds.

552 References

- 553 1. **Frayssinet S.** *Colletotrichum destructivum*: a new lucerne pathogen in Argentina. *Australasian*
554 *Plant Disease Notes* 2008 3:1 2008;3:68–68.
- 555 2. **Latunde-Dada AO, Bailey JA, Lucas JA.** Infection process of *Colletotrichum destructivum* O’Gara
556 from lucerne (*Medicago sativa* L.). *European Journal of Plant Pathology* 1997;103:35–41.
- 557 3. **Damm U, O’Connell RJ, Groenewald JZ, Crous PW.** The *Colletotrichum destructivum* species
558 complex – hemibiotrophic pathogens of forage and field crops. *Studies in Mycology* 2014;79:49–
559 84.
- 560 4. **Sun HY, Liang Y.** First report of anthracnose on sunflower caused by *Colletotrichum destructivum*
561 in China. *Plant Disease* 2018;102:245.

- 562 5. **Manandhar JB.** *Colletotrichum destructivum*, the anamorph of *Glomerella glycines*.
563 *Phytopathology* 1986;76:282.
- 564 6. **Tiffany LH, Gilman JC.** Species of *Colletotrichum* from Legumes. *Mycologia* 1954;46:52–75.
- 565 7. **Damm U, Sato T, Alizadeh A, Groenewald JZ, Crous P.** The *Colletotrichum dracaenophilum*, *C.*
566 *magnum* and *C. orchidearum* species complexes. *Studies in mycology*;92. 2019. DOI:
567 10.1016/J.SIMYCO.2018.04.001.
- 568 8. **Gan P, Tsushima A, Hiroyama R, Narusaka M, Takano Y, et al.** *Colletotrichum shiso* sp. nov., an
569 anthracnose pathogen of *Perilla frutescens* in Japan: molecular phylogenetic, morphological and
570 genomic evidence. *Scientific Reports*;9. 2019. DOI: 10.1038/s41598-019-50076-5.
- 571 9. **Dallery J-F, Lapalu N, Zampounis A, Pigné S, Luyten I, et al.** Gapless genome assembly of
572 *Colletotrichum higginsianum* reveals chromosome structure and association of transposable
573 elements with secondary metabolite gene clusters. *BMC Genomics* 2017;18:667.
- 574 10. **Tsushima A, Gan P, Kumakura N, Narusaka M, Takano Y, et al.** Genomic plasticity mediated by
575 transposable elements in the plant pathogenic fungus *Colletotrichum higginsianum*. *Genome*
576 *biology and evolution* 2019;11:1487–1500.
- 577 11. **Lelwala R V., Korhonen PK, Young ND, Scott JB, Ades PK, et al.** Comparative genome analysis
578 indicates high evolutionary potential of pathogenicity genes in *Colletotrichum tanacetii*. *PLOS*
579 *ONE* 2019;14:e0212248.
- 580 12. **Bhadoria V, MacLachlan R, Pozniak C, Cohen-Skalie A, Li L, et al.** Genetic map-guided genome
581 assembly reveals a virulence-governing minichromosome in the lentil anthracnose pathogen
582 *Colletotrichum lentis*. *The New phytologist* 2019;221:431–445.
- 583 13. **Wang Haoming, Huang Rong, Ren Jingyi, Tang Lihua, Huang Suiping, et al.** The evolution of
584 mini-chromosomes in the fungal genus *Colletotrichum*. *mBio* 2023;14:e00629-23.
- 585 14. **Plaumann P-L, Koch C.** The many questions about mini chromosomes in *Colletotrichum spp.*
586 *Plants*;9. 2020. DOI: 10.3390/plants9050641.
- 587 15. **Ma LJ, Van Der Does HC, Borkovich KA, Coleman JJ, Daboussi MJ, et al.** Comparative genomics
588 reveals mobile pathogenicity chromosomes in *Fusarium*. *Nature* 2010 464:7287 2010;464:367–
589 373.
- 590 16. **Liu S, Lin G, Ramachandran SR, Daza LC, Cruppe G, et al.** Rapid mini-chromosome divergence
591 among fungal isolates causing wheat blast outbreaks in Bangladesh and Zambia. *New*
592 *Phytologist*. 2023. DOI: 10.1111/nph.19402.
- 593 17. **Plaumann P-L, Schmidpeter J, Dahl M, Taher L, Koch C.** A dispensable chromosome is required
594 for virulence in the hemibiotrophic plant pathogen *Colletotrichum higginsianum*. *Frontiers in*
595 *microbiology* 2018;9:1005.
- 596 18. **O’Connell R, Herbert C, Sreenivasaprasad S, Khatib M, Esquerré-Tugayé M-T, et al.** A novel
597 *Arabidopsis-Colletotrichum* pathosystem for the molecular dissection of plant-fungal
598 interactions. *Molecular plant-microbe interactions : MPMI* 2004;17:272–82.
- 599 19. **Stiehler F, Steinborn M, Scholz S, Dey D, Weber APM, et al.** Helixer: cross-species gene
600 annotation of large eukaryotic genomes using deep learning. *Bioinformatics* 2021;36:5291–5298.

- 601 20. **Koren S, Walenz BP, Berlin K, Miller JR, Bergman NH, et al.** Canu: scalable and accurate long-
602 read assembly via adaptive k-mer weighting and repeat separation. *Genome research*
603 2017;27:722–736.
- 604 21. **Seppey M, Manni M, Zdobnov EM.** BUSCO: Assessing genome assembly and annotation
605 completeness. In: *Methods in Molecular Biology*. Humana Press Inc.; 2019. pp. 227–245.
- 606 22. **Rehmeyer C, Li W, Kusaba M, Kim Y-S, Brown D, et al.** Organization of chromosome ends in the
607 rice blast fungus, *Magnaporthe oryzae*. *Nucleic Acids Research* 2006;34:4685–4701.
- 608 23. **Soorni A, Haak D, Zaitlin D, Bombarely A.** Organelle_PBA, a pipeline for assembling chloroplast
609 and mitochondrial genomes from PacBio DNA sequencing data. *BMC genomics* 2017;18:49.
- 610 24. **Bolger AM, Lohse M, Usadel B.** Trimmomatic: a flexible trimmer for Illumina sequence data.
611 *Bioinformatics (Oxford, England)* 2014;30:2114–20.
- 612 25. **Dobin A, Davis CA, Schlesinger F, Drenkow J, Zaleski C, et al.** STAR: ultrafast universal RNA-seq
613 aligner. *Bioinformatics* 2013;29:15–21.
- 614 26. **Flutre T, Duprat E, Feuillet C, Quesneville H.** Considering transposable element diversification in
615 *de novo* annotation approaches. *PLoS one* 2011;6:e16526.
- 616 27. **Amselem J, Lebrun M-H, Quesneville H.** Whole genome comparative analysis of transposable
617 elements provides new insight into mechanisms of their inactivation in fungal genomes. *BMC*
618 *genomics* 2015;16:141.
- 619 28. **Hoede C, Arnoux S, Moisset M, Chaumier T, Inizan O, et al.** PASTEC: an automatic transposable
620 element classification tool. *PLoS ONE* 2014;9:e91929.
- 621 29. **Wicker T, Sabot F, Hua-Van A, Bennetzen JL, Capy P, et al.** A unified classification system for
622 eukaryotic transposable elements. *Nature Reviews Genetics* 2007;8:973–982.
- 623 30. **Sallet E, Gouzy J, Schiex T.** EuGene: An automated integrative gene finder for eukaryotes and
624 prokaryotes. Humana, New York, NY; 2019. pp. 97–120.
- 625 31. **Min B, Grigoriev I V, Choi I-G.** FunGAP: fungal genome annotation pipeline using evidence-based
626 gene model evaluation. *Bioinformatics* 2017;33:2936–2937.
- 627 32. **Eilbeck K, Moore B, Holt C, Yandell M.** Quantitative measures for the management and
628 comparison of annotated genomes. *BMC bioinformatics* 2009;10:67.
- 629 33. **Valach M, Burger G, Gray MW, Lang BF.** Widespread occurrence of organelle genome-encoded
630 5S rRNAs including permuted molecules. *Nucleic acids research* 2014;42:13764–77.
- 631 34. **Bernt M, Donath A, Jühling F, Externbrink F, Florentz C, et al.** MITOS: improved *de novo*
632 metazoan mitochondrial genome annotation. *Molecular Phylogenetics and Evolution*
633 2013;69:313–319.
- 634 35. **Drillon G, Carbone A, Fischer G.** SynChro: a fast and easy tool to reconstruct and visualize
635 synteny blocks along eukaryotic chromosomes. *PLoS ONE* 2014;9:e92621.
- 636 36. **Gilchrist CLM, Chooi YH.** clinker & clustermap.js: automatic generation of gene cluster
637 comparison figures. *Bioinformatics (Oxford, England)* 2021;37:2473–2475.

- 638 37. **Jones P, Binns D, Chang H-Y, Fraser M, Li W, et al.** InterProScan 5: genome-scale protein
639 function classification. *Bioinformatics* 2014;30:1236.
- 640 38. **Camacho C, Coulouris G, Avagyan V, Ma N, Papadopoulos J, et al.** BLAST+: architecture and
641 applications. *BMC Bioinformatics* 2009;10:421.
- 642 39. **Gene Ontology Consortium.** The Gene Ontology (GO) database and informatics resource. *Nucleic
643 Acids Research* 2004;32:258D – 261.
- 644 40. **Götz S, García-Gómez JM, Terol J, Williams TD, Nagaraj SH, et al.** High-throughput functional
645 annotation and data mining with the Blast2GO suite. *Nucleic Acids Research* 2008;36:3420.
- 646 41. **Zhang H, Yohe T, Huang L, Entwistle S, Wu P, et al.** dbCAN2: a meta server for automated
647 carbohydrate-active enzyme annotation. *Nucleic Acids Research* 2018;46:W95–W101.
- 648 42. **Petersen TN, Brunak S, von Heijne G, Nielsen H.** SignalP 4.0: discriminating signal peptides from
649 transmembrane regions. *Nature Methods* 2011;8:785–786.
- 650 43. **Emanuelsson O, Nielsen H, Brunak S, von Heijne G.** Predicting subcellular localization of proteins
651 based on their N-terminal amino acid sequence. *Journal of Molecular Biology* 2000;300:1005–
652 1016.
- 653 44. **Krogh A, Larsson B, von Heijne G, Sonnhammer ELL.** Predicting transmembrane protein
654 topology with a hidden markov model: application to complete genomes. *Journal of Molecular
655 Biology* 2001;305:567–580.
- 656 45. **Sperschneider J, Dodds PN, Gardiner DM, Singh KB, Taylor JM.** Improved prediction of fungal
657 effector proteins from secretomes with EffectorP 2.0. *Molecular plant pathology* 2018;19:2094–
658 2110.
- 659 46. **Blin K, Shaw S, Steinke K, Villebro R, Ziemert N, et al.** antiSMASH 5.0: updates to the secondary
660 metabolite genome mining pipeline. *Nucleic Acids Research* 2019;47:W81–W87.
- 661 47. **Zhou P, Silverstein KAT, Ramaraj T, Guhlin J, Denny R, et al.** Exploring structural variation and
662 gene family architecture with *de novo* assemblies of 15 *Medicago* genomes. *BMC Genomics*
663 2017;18:261.
- 664 48. **Moll KM, Zhou P, Ramaraj T, Fajardo D, Devitt NP, et al.** Strategies for optimizing BioNano and
665 Dovetail explored through a second reference quality assembly for the legume model, *Medicago
666 truncatula*. *BMC Genomics* 2017;18:578.
- 667 49. **O’Connell RJ, Thon MR, Hacquard S, Amyotte SG, Kleemann J, et al.** Lifestyle transitions in plant
668 pathogenic *Colletotrichum* fungi deciphered by genome and transcriptome analyses. *Nature
669 Genetics* 2012;44:1060–1065.
- 670 50. **Coleman JJ, Rounsley SD, Rodriguez-Carres M, Kuo A, Wasmann CC, et al.** The genome of
671 *Nectria haematococca*: contribution of supernumerary chromosomes to gene expansion. *PLOS
672 Genetics* 2009;5:e1000618.
- 673 51. **Hu J, Chen C, Peever T, Dang H, Lawrence C, et al.** Genomic characterization of the conditionally
674 dispensable chromosome in *Alternaria arborescens* provides evidence for horizontal gene
675 transfer. *BMC genomics* 2012;13:1–13.

- 676 52. **Vollger MR, Dishuck PC, Sorensen M, Welch AE, Dang V, et al.** Long-read sequence and
677 assembly of segmental duplications. *Nature Methods* 2019;16:88–94.
- 678 53. **Liu F, Ma ZY, Hou LW, Diao YZ, Wu WP, et al.** Updating species diversity of *Colletotrichum*, with
679 a phylogenomic overview. *Studies in Mycology*;101.
- 680 54. **Rogério F, Bouffleur TR, Ciampi-Guillardi M, Sukno SA, Thon MR, et al.** Genome sequence
681 resources of *Colletotrichum truncatum*, *C. plurivorum*, *C. musicola*, and *C. sojae*: four species
682 pathogenic to soybean (*Glycine max*). *Phytopathology* 2020;110:1497–1499.
- 683 55. **Langner T, Harant A, Gomez-Luciano LB, Shrestha RK, Win J, et al.** Genomic rearrangements
684 generate hypervariable mini-chromosomes in host-specific lineages of the blast fungus. *bioRxiv*
685 2020;2020.01.10.901983.
- 686 56. **Langner T, Harant A, Gomez-Luciano LB, Shrestha RK, Malmgren A, et al.** Genomic
687 rearrangements generate hypervariable mini-chromosomes in host-specific isolates of the blast
688 fungus. *PLOS Genetics* 2021;17:e1009386.
- 689 57. **Vanheule A, Audenaert K, Warris S, van de Geest H, Schijlen E, et al.** Living apart together:
690 crosstalk between the core and supernumerary genomes in a fungal plant pathogen. *BMC*
691 *Genomics* 2016;17:1–18.
- 692 58. **Condon BJ, Leng Y, Wu D, Bushley KE, Ohm RA, et al.** Comparative genome structure, secondary
693 metabolite, and effector coding capacity across *Cochliobolus* pathogens. *PLoS Genetics*
694 2013;9:e1003233.
- 695 59. **Yang G, Turgeon BG, Yoder OC, Bronson CR, Yoder OC, et al.** Toxin-deficient mutants from a
696 toxin-sensitive transformant of *Cochliobolus heterostrophus*. *Genetics* 1994;137:751–7.
- 697 60. **Klosterman SJ, Subbarao K V., Kang S, Veronese P, Gold SE, et al.** Comparative genomics yields
698 insights into niche adaptation of plant vascular wilt pathogens. *PLOS Pathogens*
699 2011;7:e1002137.
- 700 61. **Gan P, Hiroyama R, Tsushima A, Masuda S, Shibata A, et al.** Telomeres and a repeat-rich
701 chromosome encode effector gene clusters in plant pathogenic *Colletotrichum* fungi.
702 *Environmental Microbiology* 2021;23:6004–6018.
- 703 62. **Croll D, Zala M, McDonald BA.** Breakage-fusion-bridge cycles and large insertions contribute to
704 the rapid evolution of accessory chromosomes in a fungal pathogen. *PLOS Genetics*
705 2013;9:e1003567.
- 706 63. **Bertazzoni S, Williams AH, Jones DA, Syme RA, Tan K-C, et al.** Accessories make the outfit:
707 accessory chromosomes and other dispensable DNA regions in plant-pathogenic fungi. *Molecular*
708 *Plant-Microbe Interactions* 2018;31:779–788.
- 709 64. **Francis A, Ghosh S, Tyagi K, Prakasam V, Rani M, et al.** Evolution of pathogenicity-associated
710 genes in *Rhizoctonia solani* AG1-IA by genome duplication and transposon-mediated gene
711 function alterations. *BMC Biology* 2023;21:1–19.
- 712 65. **Fraser JA, Huang JC, Pukkila-Worley R, Alspaugh JA, Mitchell TG, et al.** Chromosomal
713 translocation and segmental duplication in *Cryptococcus neoformans*. *Eukaryotic Cell*
714 2005;4:401–406.

- 715 66. **van Westerhoven A, Aguilera-Galvez C, Nakasato-Tagami G, Shi-Kunne X, Martinez E, et al.**
716 Segmental duplications drive the evolution of accessory regions in a major crop pathogen.
717 *bioRxiv* 2023;2023.06.07.544053.
- 718 67. **Wilson AM, Lelwala R V., Taylor PWJ, Wingfield MJ, Wingfield BD.** Unique patterns of mating
719 pheromone presence and absence could result in the ambiguous sexual behaviors of
720 *Colletotrichum* species. *G3 Genes/Genomes/Genetics*;11. 2021. DOI:
721 10.1093/G3JOURNAL/JKAB187.
- 722 68. **Bhunjun CS, Phukhamsakda C, Jeewon R, Promputtha I, Hyde KD.** Integrating different lines of
723 evidence to establish a novel Ascomycete genus and family (*Anastomitrabeculia*,
724 *Anastomitrabeculiaceae*) in Pleosporales. *Journal of Fungi* 2021, Vol 7, Page 94 2021;7:94.
- 725 69. **Manners JM, He C.** Slow-growing heterokaryons as potential intermediates in supernumerary
726 chromosome transfer between biotypes of *Colletotrichum gloeosporioides*. *Mycological Progress*
727 2011;10:383–388.
- 728 70. **He C, Rusu AG, Poplawski AM, Irwin JAG, Manners JM.** Transfer of a supernumerary
729 chromosome between vegetatively incompatible biotypes of the fungus *Colletotrichum*
730 *gloeosporioides*. *Genetics* 1998;150:1459–1466.
- 731 71. **Roca MG, Davide LC, Davide LMC, Mendes-Costa MC, Schwan RF, et al.** Conidial anastomosis
732 fusion between *Colletotrichum* species. *Mycological research* 2004;108:1320–1326.
- 733 72. **Ishikawa FH, Souza EA, Shoji JY, Connolly L, Freitag M, et al.** Heterokaryon incompatibility is
734 suppressed following conidial anastomosis tube fusion in a fungal plant pathogen. *PLoS one*;7.
735 2012. DOI: 10.1371/JOURNAL.PONE.0031175.
- 736 73. **Mehta N, Baghela A.** Quorum sensing-mediated inter-specific conidial anastomosis tube fusion
737 between *Colletotrichum gloeosporioides* and *C. siamense*. *IMA fungus*;12. 2021. DOI:
738 10.1186/S43008-021-00058-Y.
- 739 74. **Schmidt SM, Houterman PM, Schreiver I, Ma L, Amyotte S, et al.** MITEs in the promoters of
740 effector genes allow prediction of novel virulence genes in *Fusarium oxysporum*. *BMC genomics*
741 2013;14:1–21.
- 742 75. **van der Does HC, Fokkens L, Yang A, Schmidt SM, Langereis L, et al.** Transcription factors
743 encoded on core and accessory chromosomes of *Fusarium oxysporum* induce expression of
744 effector genes. *PLOS Genetics* 2016;12:e1006401.
- 745 76. **Mould MJR, Boland GJ, Robb J.** Ultrastructure of the *Colletotrichum trifolii-Medicago sativa*
746 pathosystem. I. Pre-penetration events. *Physiological and Molecular Plant Pathology*
747 1991;38:179–194.
- 748 77. **Damm U, Cannon PF, Liu F, Barreto RW, Guatimosim E, et al.** The *Colletotrichum orbiculare*
749 species complex: Important pathogens of field crops and weeds. *Fungal Diversity* 2013;61:29–59.
- 750 78. **C A-T, BB W, MS O, S D, H Z, et al.** Identification and characterization of nucleotide-binding site-
751 leucine-rich repeat genes in the model plant *Medicago truncatula*. *Plant physiology*;146. 2008.
752 DOI: 10.1104/PP.107.104588.

753

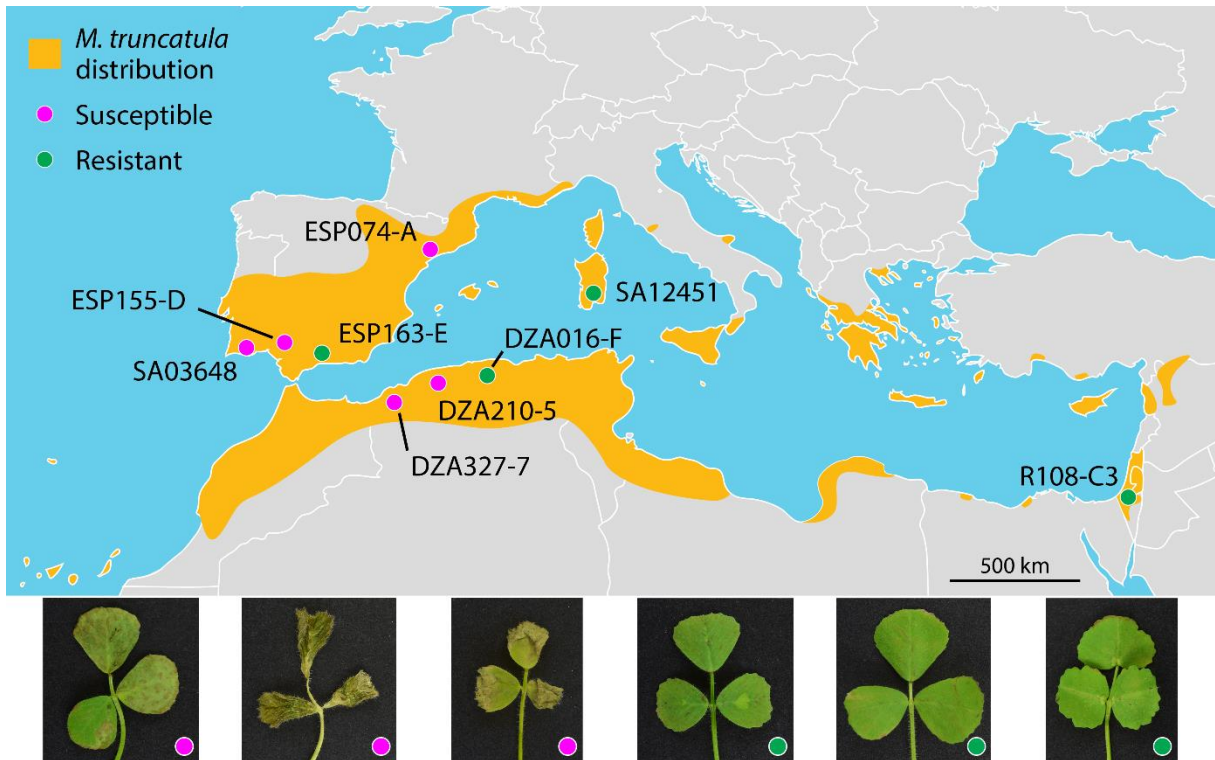
754 **Table 1:** Characteristics of *C. destructivum* core and mini chromosomes.

	<i>C. destructivum</i> chromosomes			
	1-10 (except 1B)	1B region	11	12
Total length	48 456 982 bp	1 205 667 bp	1 275 594 bp	812 569 bp
G+C content	54.7 %	52.3 %	48.7 %	50.2 %
Number of protein-coding genes	14882	300	278	171
Proportion of genes by length	61.7 %	30.9 % ^{***}	32.3 % ^{***}	26.8 % ^{***}
Proportion of genes with unknown function	21.3 %	42.0 % ^{***}	28.4 % [*]	32.2 % [*]
Proportion of genes with RNA support	77.0 %	52.0 % ^{***}	46.4 % ^{***}	59.6 % [*]
Proportion of CAZyme genes	4.1 %	0.0 % ^{***}	1.4 %	1.2 %
Proportion of effector genes	3.0 %	4.3 %	5.4 % [*]	5.8 % [*]
Proportion of SMKG	0.7 %	0.0 %	2.9 % ^{**}	0.0 %
Proportion of TE by length	4.4 %	32.8 % ^{***}	32.3 % ^{***}	35.1 % ^{***}

755 Asterisks indicate that the data for chromosomes 1B, 11 or 12 differ significantly from the core chromosomes (Fisher's
 756 exact test, *** $P < 0.001$; ** $P < 0.01$; * $P < 0.05$)

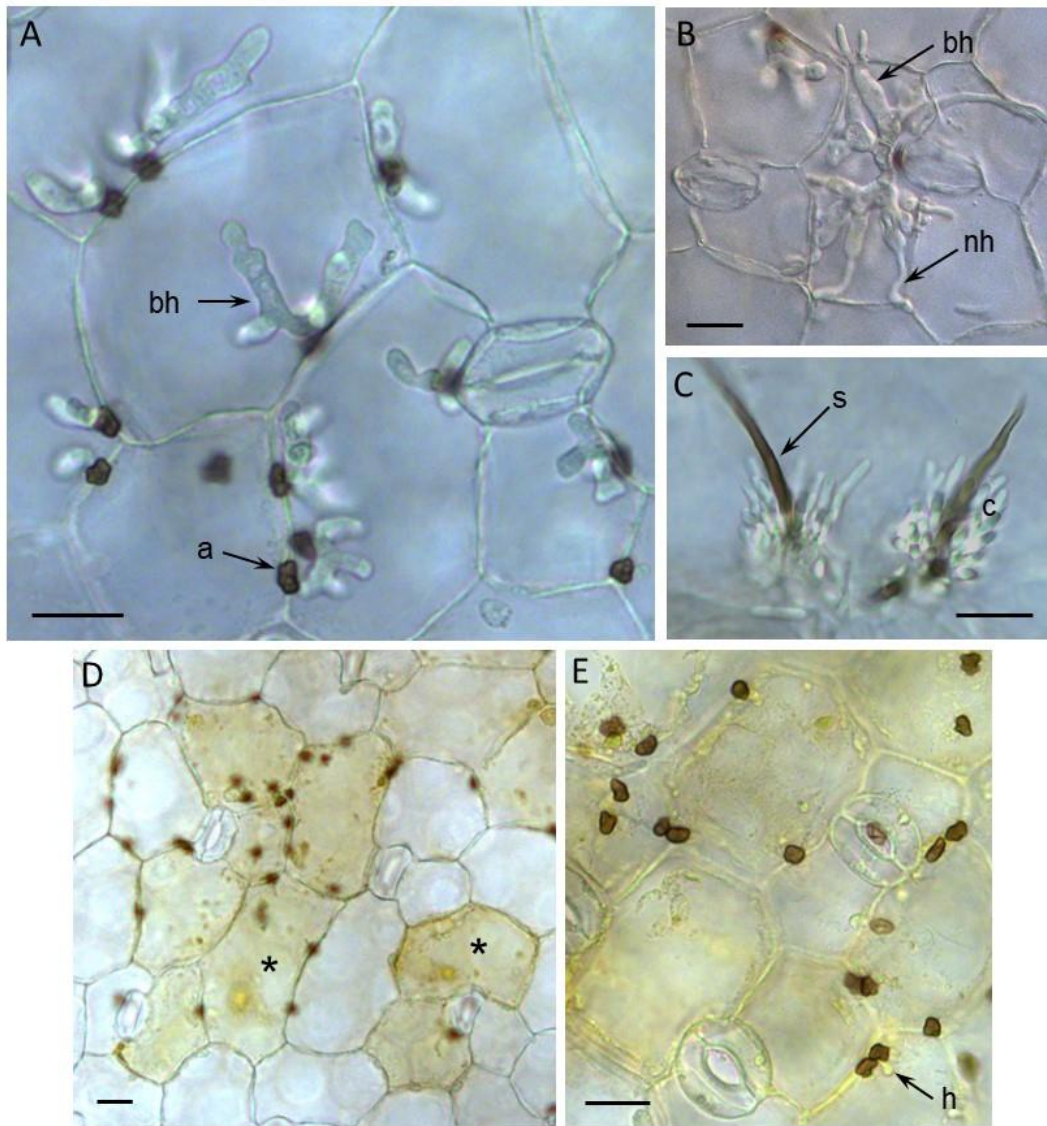
757

758

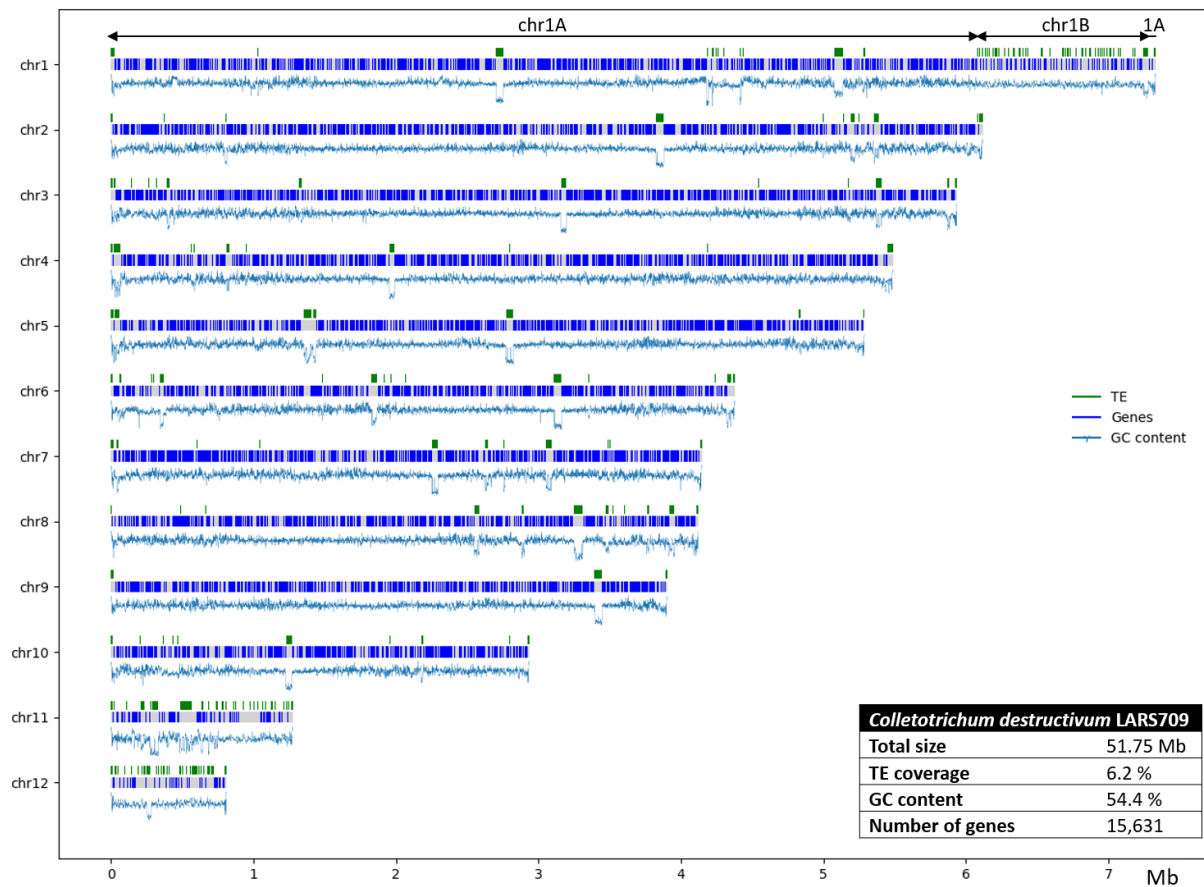


759
760
761
762
763
764
765
766
767
768
769

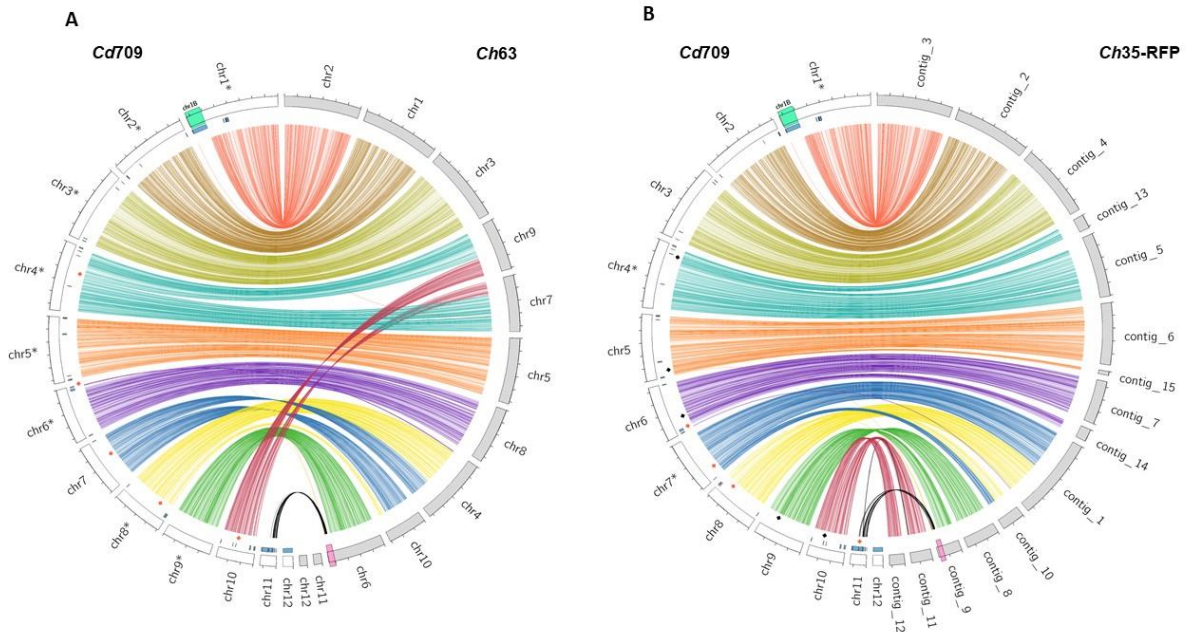
Figure 1: *Medicago truncatula* accessions used in this study and their infection phenotypes with *Colletotrichum destructivum* LARS 709. Upper panel: Geographical distribution of *M. truncatula* in the Mediterranean area according to GBIF (2019) and collection locations of the nine ecotypes used in this study. **Lower panel:** Symptoms produced on the trifoliate leaves of six *M. truncatula* accessions at 4 days post inoculation with spore suspension of *C. destructivum* LARS 709. Leaves of the susceptible accession DZA210-5 showed large necrotic lesions, while those of DZA327-7 and ESP155-D were completely necrotic. Leaves of the resistant accessions ESP163-E, DZA016-F and R108-C3 showed small necrotic flecks or no visible symptoms. Note that R108-C3 is considered to be *M. truncatula* ssp. *tricycla*.



770
 771 **Figure 2: Microscopic analysis of *Colletotrichum destructivum* LARS 709 infecting cotyledon tissues**
 772 **of *Medicago truncatula*.** (A-C) Susceptible accession ESP155-D. At 48 hpi (A), melanized appressoria
 773 (a) had formed on the plant surface and penetrated epidermal cells to form bulbous biotrophic hyphae
 774 (bh). At 60 hpi (B), thin necrotrophic hyphae (nh) developed from the tips of biotrophic hyphae. At 72
 775 hpi (C), acervuli erupted from the plant surface, consisting of a melanized, hair-like seta (s) and a mass
 776 of conidia (c). (D,E) Resistant accession ESP163-E. At 72 hpi, few appressoria had penetrated cotyledon
 777 epidermal cells, and groups of cells underlying the appressoria were pigmented yellowish brown with
 778 granular contents (*). Any hyphae (h) visible inside epidermal cells were typically smaller than the
 779 appressorium. Scale bars = 20 μ m.
 780

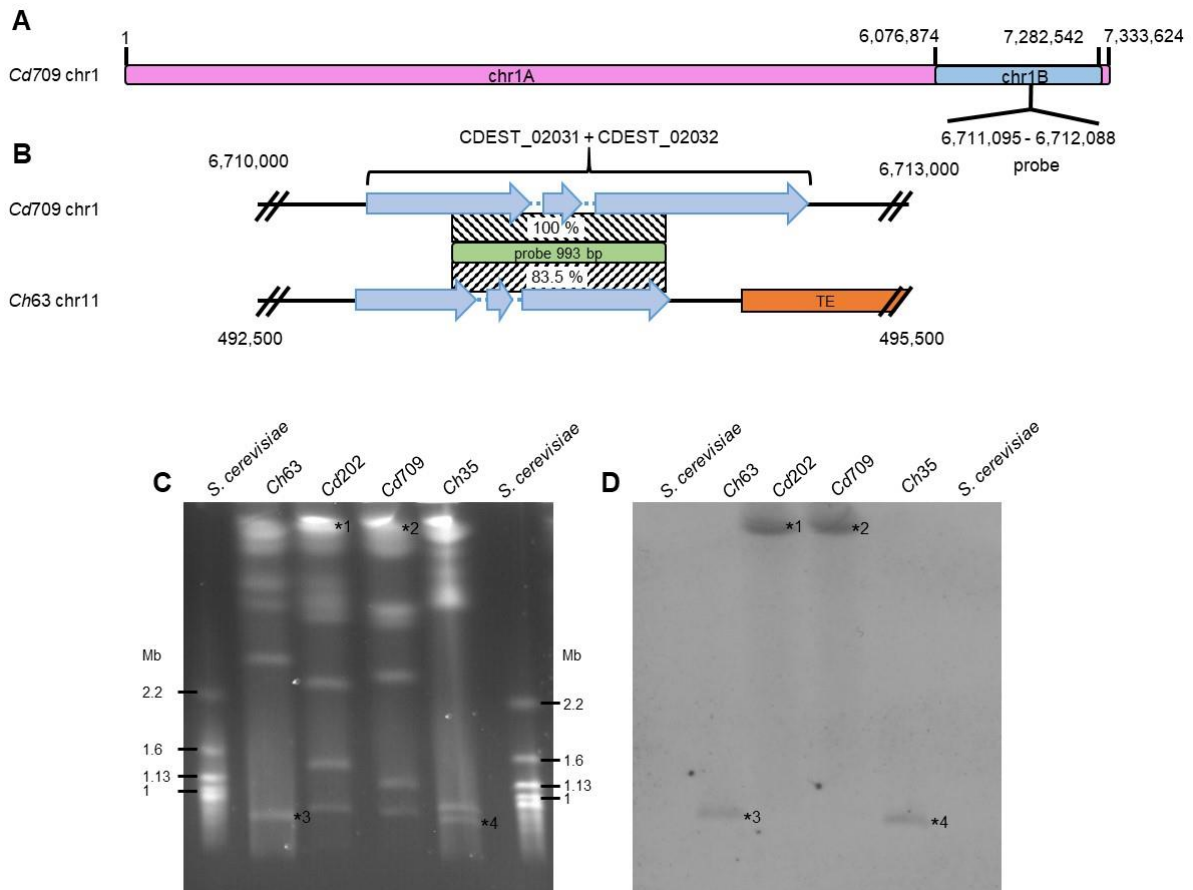


781
 782 **Figure 3: Schematic representation of the 12 chromosomes of *Colletotrichum destructivum* isolate**
 783 **709.** The distribution of genes and transposable elements (TE) across each chromosome are shown
 784 together with the corresponding genome statistics (inset table).
 785

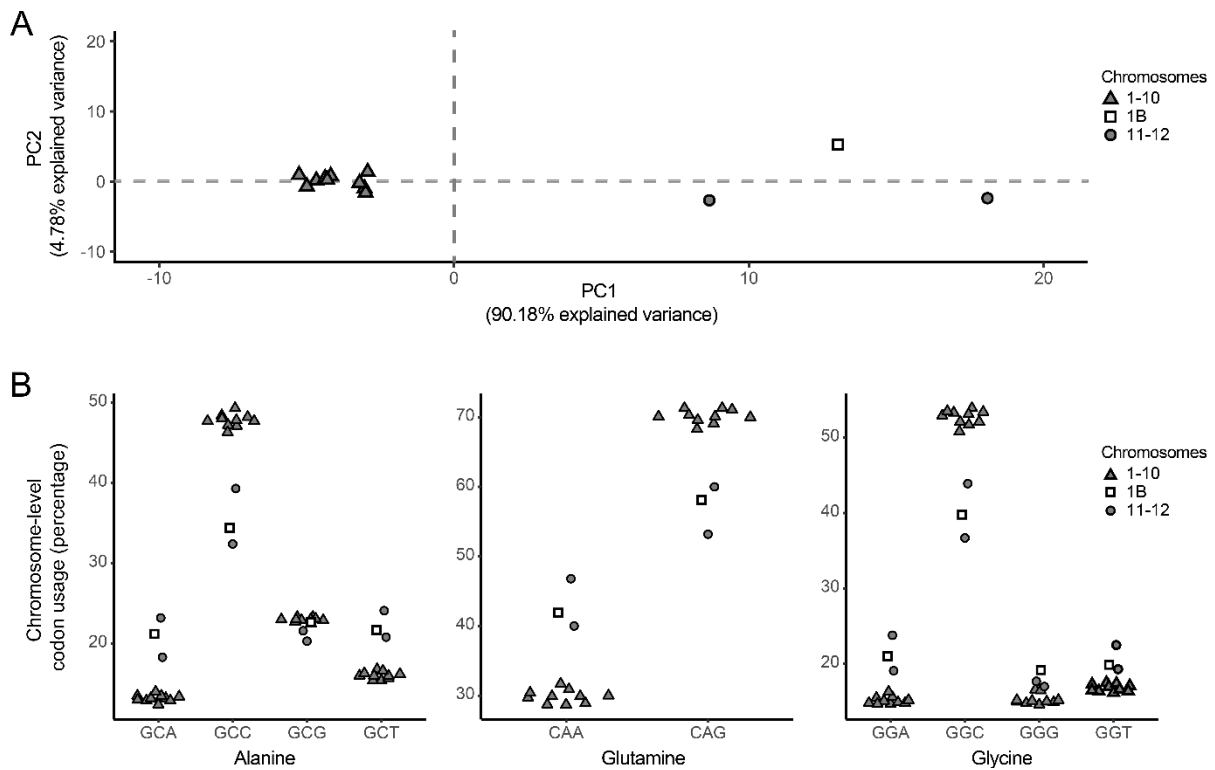


786
 787
 788
 789
 790
 791
 792
 793
 794
 795
 796
 797
 798
 799
 800

Figure 4: Whole-genome alignments between *Colletotrichum destructivum* LARS 709 (Cd709) and two *Colletotrichum higginsianum* strains. Chromosomes of Cd709 (white bars) were aligned with **(A)** the chromosomes of *C. higginsianum* IMI 349063 (Ch63, grey bars) or **(B)** the contigs of *C. higginsianum* MAFF 304535-RFP (Ch35-RFP, grey bars). Syntenic regions (length >10 kb and percent identity > 88%) were linked together using coloured arcs specific for each chromosome in the Cd709 genome assembly. Red diamonds indicate interchromosomal rearrangements. Black diamonds indicate chromosome breakpoints associated with separate contigs in the Ch35-RFP assembly only. The blue track indicates gene blocks that are unique to Cd709. Note that region chr1B of Cd709 (highlighted in green) has no alignments in either of the *C. higginsianum* isolates. The black arcs linking chr11 of Cd709 to the 3' end of chr6/contig_9 in *C. higginsianum* (highlighted in pink) indicate regions with strong sequence similarity (percent identity > 88%) that are smaller than 10 Kb. Asterisks indicate where chromosome sequences were reverse-complemented for better visualization. Tick mark spacing = 1 Mb

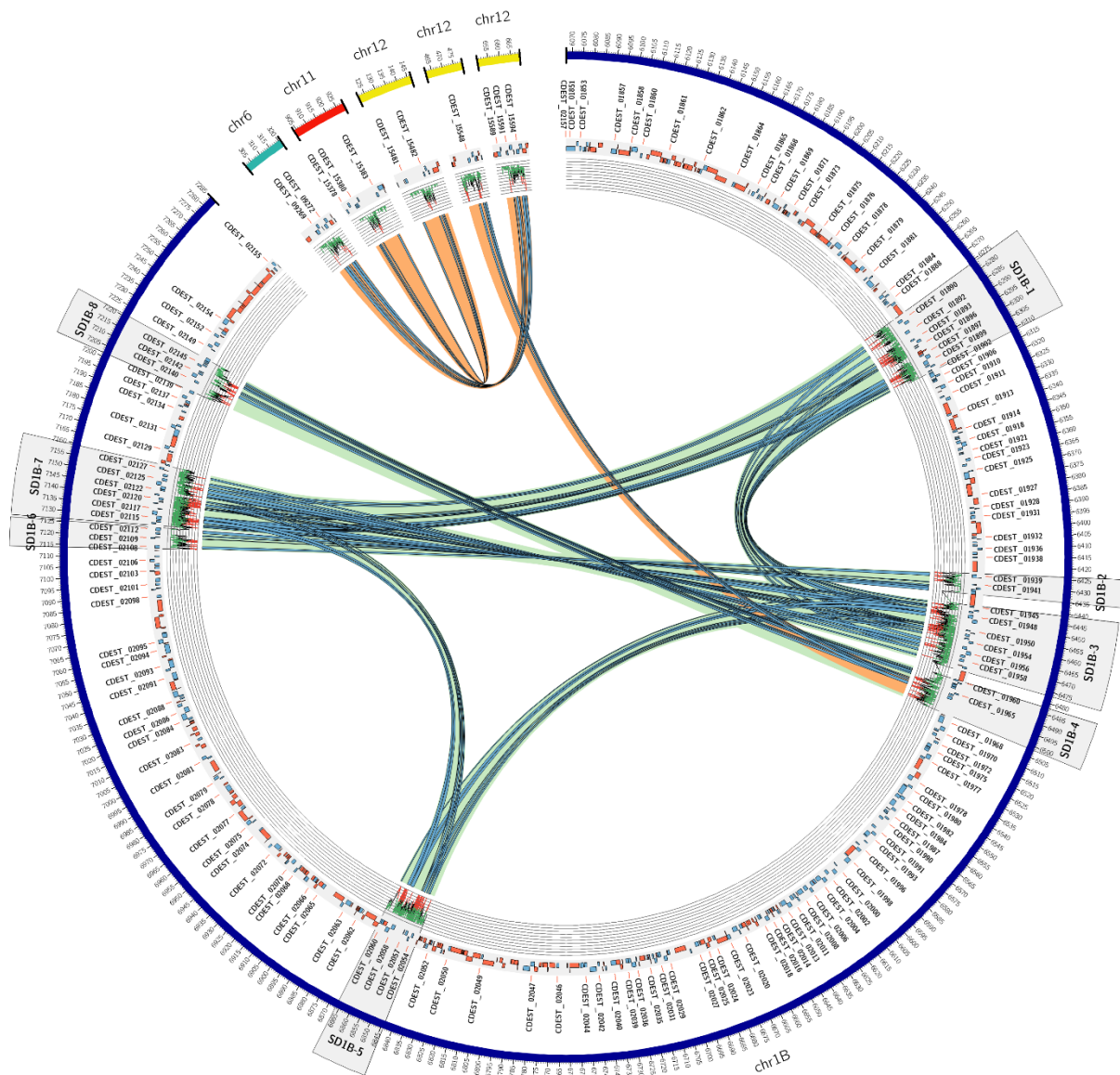


801
 802 **Figure 5: Chromosome 1 of *Colletotrichum destructivum* has a bipartite structure.** (A) Scheme of the
 803 structure of *Cd709* chromosome 1. The probe is specific to the mini-chromosome-like part of the
 804 chromosome (chr1B). (B) Detailed scheme of the regions targeted by the 993 bp DIG-labelled probe in
 805 *Cd709* and in *Ch63* (chr11: 493,380 to 494,373). Patterned boxes indicate sequence identity of the
 806 target regions to the probe. (C) Pulsed-field gel electrophoresis of chromosomal DNA from *C.*
 807 *destructivum* isolates LARS 202 (*Cd202*) and LARS 709 (*Cd709*) compared to *C. higginsianum* isolates
 808 IMI349063 (*Ch63*) and MAFF305635 (*Ch35*). (D) Southern hybridisation. Numerals 1 to 4 indicate
 809 signals corresponding to chromosomes displayed in (C).
 810



811
812
813
814
815
816
817
818
819
820
821

Figure 6: Codon usage bias in the core and mini-chromosomes of *C. destructivum*. (A) Principal component analysis (PCA) of codon usage for all amino acids on each chromosome. The region chr1B was considered separately from the rest of chr1. The first two axes accounted for 95% of the variance. (B) Plots showing codon usage bias for three amino acids (Alanine, Glutamine, Glycine) in genes located on core chromosomes (1 to 10 excluding region 1B), mini-chromosomes 11 and 12 and region 1B. Codon usage on chr11, chr12 and region chr1B differed significantly from that on core chromosomes (Fisher's exact test, $P < 0.001$) for the 10 codons presented except GCG (all comparisons) and GGG (chr12 vs core). Other amino acids are displayed in Fig. S6. The significance is reported for all the codons in the Table S12.



822
 823 **Figure 7: Circos plot showing *Colletotrichum destructivum* segmental duplications larger than 10kb**
 824 **found with SDDetector.** The green and red tracks represent genes and transposable elements
 825 respectively. The light green and orange arcs indicate intra-chromosomal and inter-chromosomal
 826 duplications respectively. Duplicated genes are highlighted by blue arcs. The level of sequence
 827 similarity along the duplications is shown by a line graph with a colour scale where green indicates
 828 greater than 95% similarity, black between 95 and 90% similarity and red below 90% similarity. A sliding
 829 window of 100 base pairs was used to calculate and display sequence similarity from large alignments.
 830 The scale displayed on the graph ranges from 100% to 85% similarity.